Downward particle fluxes of biogenic matter and Saharan dust across the equatorial North Atlantic

Laura F. Korte[1], Geert-Jan A. Brummer[1,2], Michèlle van der Does[1], Catarina V. Guerreiro[3], Rick Hennekam[1], Johannes A. van Hateren[1,2], Dirk Jong[1], Chris I. Munday[1], Stefan Schouten[4], Jan-Berend W. Stuut[1,5]

[1] NIOZ – Royal Netherlands Institute for Sea Research, Department of Ocean Systems, and Utrecht University, Texel, the Netherlands
[2] Faculty of Earth and Life Sciences, Vrije Universiteit Amsterdam, the Netherlands
[3] University of Bremen, Faculty of Earth Sciences, Bremen, Germany
[4] NIOZ – Royal Netherlands Institute for Sea Research, Department of Marine Microbiology and Biogeochemistry, and Utrecht University, Texel, the Netherlands
[5] MARUM – Center for Marine Environmental Sciences, University of Bremen, Germany

Correspondence to: Laura F. Korte (laura.korte@nioz.nl)

Abstract. Massive amounts of Saharan dust are blown from the coast of northern Africa across the Atlantic Ocean towards the Americas each year. This dust has, depending on its chemistry, direct and indirect effects on global climate including reflection and absorption of solar radiation as well as transport and deposition of nutrients and metals fertilizing both ocean and land. To determine the temporal and spatial variability of Saharan dust transport and deposition and their marine environmental effects across the equatorial North Atlantic Ocean, we have set up a monitoring experiment using deep-ocean sediment traps as well as land-based dust collectors. The sediment traps were deployed at five ocean sites along a transatlantic transect between northwest Africa and the Caribbean along 12° N, in a down-wind extension of the land-based dust collectors placed at 19° N on the Mauritanian coast in Iwik. In this paper, we lay out the setup of the monitoring experiment and present the particle fluxes from sediment trap sampling over 24 continuous and synchronised intervals from October 2012 through to November 2013. We establish the temporal distribution of the particle fluxes deposited in the Atlantic and compare chemical compositions with the land-based dust collectors propagating to the down-wind sediment trap sites, and with satellite observations of Saharan dust outbreaks.

First-year results show that the total mass fluxes in the ocean are highest at the sampling sites in the east and west, closest to the African continent and the Caribbean, respectively. Element ratios reveal that the lithogenic particles deposited nearest to Africa are most similar in composition to the Saharan dust collected in Iwik. Down-wind increasing Al, Fe and K contents suggest a downwind change in the mineralogical composition of Saharan dust and indicate an increasing contribution of clay minerals towards the west. In the westernmost Atlantic Ocean, admixture of re-suspended clay-sized sediments advected towards the deep sediment trap cannot be excluded. Seasonality is most prominent near both continents but generally weak, with mass fluxes dominated by calcium carbonate and clear seasonal maxima of biogenic silica towards the west. The monitoring experiment is now extended with autonomous dust sampling buoys for better quantification of Saharan dust transport and deposition from source to sink and its impact on fertilization and carbon export to the deep ocean.

Keywords Saharan dust; North Atlantic Ocean; sediment traps; particle fluxes; XRF element ratios; trans-Atlantic

1 Introduction

Latest estimates of transatlantic Saharan-dust transport and deposition based on 3-D satellite imagery indicate that on a yearly basis (2007 – 2013, between 10° S and 30° N) an average amount of 182 Tg dust is blown from the northwest African coast at 15°W westward towards the Americas (Yu et al., 2015). Of this dust, about 132 Tg reaches 35° W and 43 Tg reaches 75° W (Yu et al., 2015). Due to the dust's impact on global climate (e.g. Mahowald et al., 2014;Jickells et al., 2005;Griffin et al., 2001;Goudie and Middleton, 2001;Maher et al., 2010), Saharan dust has been examined extensively on either side of the equatorial North Atlantic Ocean, using ample different approaches. At the eastern side, northwest African *in-situ* measurements of dust events were performed on land (e. g. Kandler et al., 2009;Kandler et al., 2011;Marticorena et al., 2010;Kaly et al., 2015;Skonieczny et al., 2011;Skonieczny et al., 2013), in addition to ship board atmospheric dust sampling (e. g. Stuut et al., 2005;Baker et al., 2003) and deep ocean sediment fluxes (e. g. Bory et al., 2002;Ratmeyer et al., 1999b;Ratmeyer et al., 1999a;Fischer and Karakas, 2009). On the other side of the ocean, Prospero and colleagues have been sampling Saharan dust mainly on Barbados since the late 1960's, resulting in the longest continuous time series of Saharan-dust sampling (Prospero et al., 1970;2014;Prospero and Lamb, 2003). All observations of Saharan dust showed a strong seasonality with higher dust concentrations during the winter season close to the dust sources in the east, and higher dust concentrations during the summer season in the Caribbean. This seasonal pattern is related to the prevailing wind systems, which are influenced by the movement of the intertropical convergence zone (ITCZ). Saharan dust is transported year-round by the north-easterly trade winds at relatively low altitudes, carrying the dust to the proximal parts of the Atlantic Ocean (Stuut et al., 2005;Pye, 1987). In winter, easterly winds transport the dust in surface winds at altitudes below three km (Chiapello et al., 1995), when the ITCZ reaches its most southern position, and the dust crosses the Atlantic Ocean in the direction of South America (Prospero et al., 2014;1981). As the ITCZ migrates northward during summer, the dust is transported by the Saharan Air Layer (SAL) at higher altitudes up to five km (Tsamalis et al., 2013), and crosses the Atlantic Ocean above the trade-wind zone in the direction of North America and the island of Barbados (Prospero et al., 1970;2014).

The knowledge of the fate of Saharan dust in between the sources and sinks is, however, limited due to the vastness of the North Atlantic Ocean, though observed by remote sensing (e. g. Liu et al., 2008;Yu et al., 2015;Huang et al., 2010) and shipboard lidar measurements (Kanitz et al. 2014). From the latest approximation (Yu et al., 2015) it can be derived that around 50 Tg a^{-1} of dust is deposited into the eastern equatorial North Atlantic Ocean, and 140 Tg a^{-1} of dust is deposited into the equatorial North Atlantic Ocean and the Caribbean Sea as well as onto parts of the Amazon rainforest. The deposited dust onto the ocean has a great influence on the particle fluxes as well (Jickells et al., 2005;Ittekkot et al., 1992;Armstrong et al., 2009). Sediment trap studies within for example the Joint Global Ocean Flux Study (JGOFS) and Biogeochemical Ocean Flux Study (BOFS), dealing with deep ocean particle fluxes, show elevated total mass fluxes with a high contribution of lithogenic particle fluxes in the North Atlantic Ocean off Mauritania (Jickells et al. 1996). In addition, Saharan dust particles are thought to contribute to the total flux in the Sargasso Sea (Deuser et al., 1988).

A 25-year time series of northwest African dust fluxes was established at the University of Bremen, Germany, using sediment traps moored on the Mauritanian continental slope. First results were presented by Wefer and Fischer (1993), Ratmeyer et al. (1999a; 1999b) and Nowald et al. (2015), followed by the 25-year record by Fischer et al. (2016). On average, lithogenic particles make up about a third of the total mass flux and up to 50 % during dust events (Nowald et al., 2015). Biogenic mass fluxes in this area are generally high as well, as the sediment traps are located in one of the four major Eastern Boundary Upwelling Ecosystems (EBUEs) (Fréon et al., 2009), bringing cold, nutrient-rich waters to the surface waters stimulating primary productivity. Fischer et al. (2016)

demonstrate that the Cape-Blanc sediment-trap series showed a weak relationship between dust input and productivity as reflected by the biogenic silica, mainly derived from diatoms as important primary producers. In addition, dust particles were found to strongly enhance the settling of organic matter through the water column by means of mineral ballasting, although no evidence was found for a relation between bulk fluxes and dust particle size.

In order to determine the simultaneous downward particle flux of the deposited Saharan dust across the entire Atlantic Ocean between the source in Africa and the sinks in the Atlantic Ocean and Caribbean Sea, we deployed an array of five moorings below the core of the dust plume, starting in 2012. Based on eight years of satellite observations, the Saharan dust plume is very consistently located between 7° and 17ºN (Mulitza et al., 2008). Therefore, the array of moorings was positioned along the 12th northern parallel between 23ºW and 57ºW, each equipped with two time-series sediment traps. In addition, we positioned land-based dust collectors in Iwik on the Mauritanian coast nearest to the source (Fig. 1). Here, we present the initial set-up of the monitoring experiment and the first-year results of the mass fluxes and their composition as intercepted by the sediment traps in the Atlantic and the land-based samplers in Iwik. The results are compared both with each other, and satellite images of atmospheric Saharan dust transport, recorded by the Moderate Resolution Imaging Spectroradiometer (MODIS) carried by the Terra satellite. Complementary results of the size distributions of Saharan dust from the sediment traps were discussed by Van der Does et al. (2016), showing a strong seasonality with coarser grained dust in summer and finer grained dust in winter and spring, as well as a fining in particle size with increasing distance to the source.

2 Instrumentation and Performance

2.1 Land-based dust collectors

Saharan dust transport and deposition is traced from source to sink, starting on the Mauritanian coast with two masts with passive modified Wilson and Cooke samplers (MWAC dust collectors; Goossens and Offer (2000), located in Iwik ($19^0$53.11'N, $16^0$17.64'W), which have been sampling dust over monthly intervals since January 2013. Each mast contains a total of ten MWAC samplers, deployed in pairs at five heights, equally spaced at 90 to 290 cm from the ground. The masts contain a wind vane that directs the opening of the MWAC collectors into the wind.
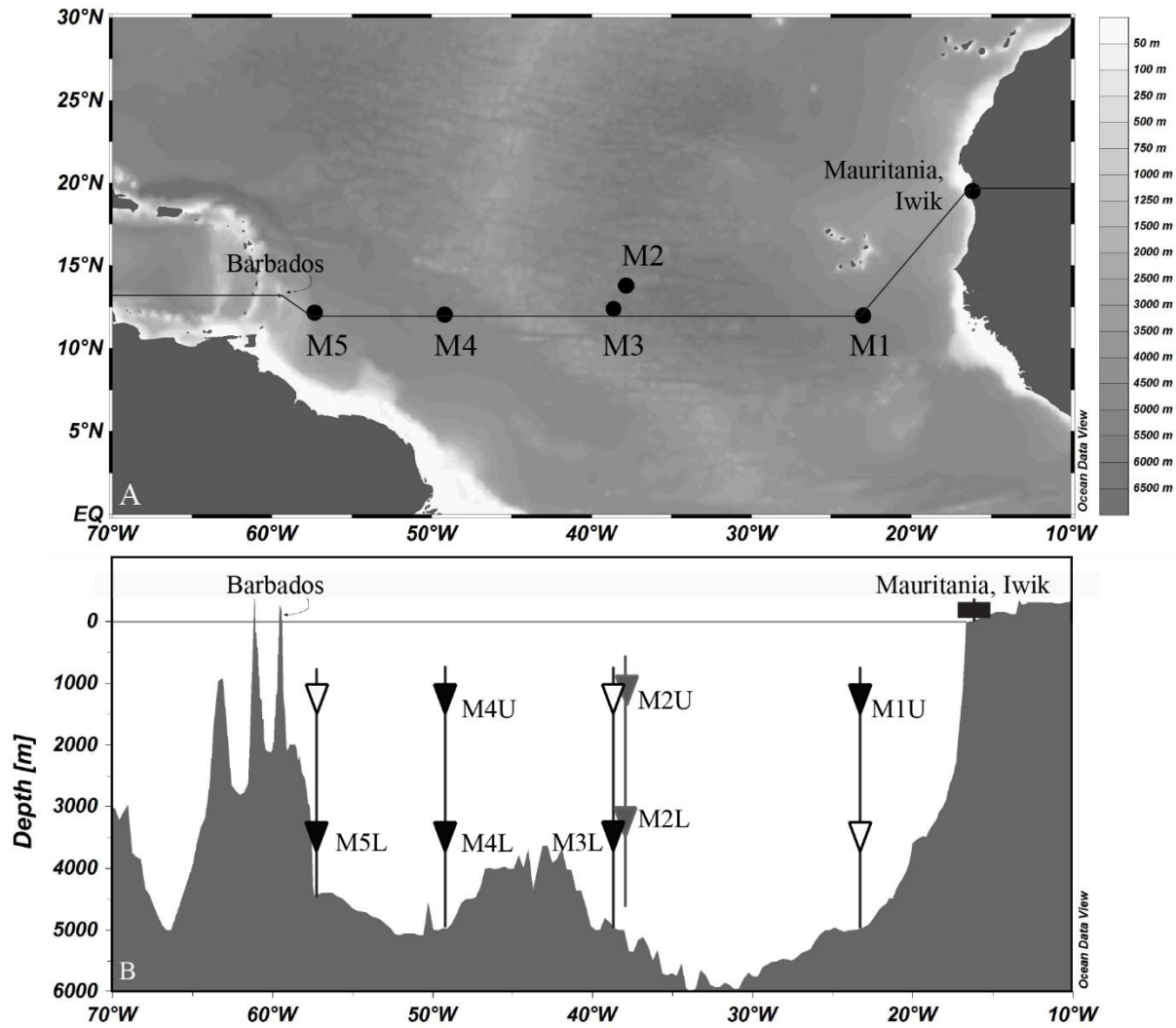
Figure. 1. A: Location of land-based dust collectors on the Mauritanian coast in the village of Iwik and sediment trap moorings M1 – M5 between northwest Africa and Barbados. B: Bathymetric profile, on the line in A, through the equatorial North Atlantic between Mauritania (15° W) and Barbados (60° W) showing the five moorings with sediment traps (triangles) and the land-based MWAC dust collectors (rectangle). MxU and MxL indicate the upper and the lower traps on the five moorings at 1200m and 3500m nominal water depth, respectively. Open symbols refer to sediment traps that failed or were lost during recovery.

2.2 Ocean moorings

Sediment traps are a common tool for direct and accurate time-series measurements of settling particles in the ocean when conditions are favourable, e.g. low currents (< 12m s^{-1}), no deep eddy penetration and a vertical mooring line (Knauer and Asper, 1989). Moorings were deployed at five sites (M1 – M5) along a transect in the equatorial North Atlantic during RV Meteor cruise M89 (Stuut et al., 2012) in October 2012 (Fig. 1). Four of the five moorings (M1, M3, M4 and M5) were deployed at 12^{0}N and 23^{0}W, 38^{0}W, 49^{0}W and 57^{0}W, respectively, and one mooring (M2) was positioned to the north of station M3 and deployed at 13.5^{0}N and 37.5 ^{0}W to assess potential north-south movements of the Saharan dust plume. Each mooring was equipped with a number of oceanographic instruments (Table 1). These include two Technicap PPS 5/2 sediment traps provided with a tilt meter at a nominal water depth of 1200 m (upper) and 3500 m (lower), two SBE MicroCat CTDs for conductivity, temperature and depth measurements, two Aanderaa RCM-11 current meters, and four floatation bodies to keep the mooring upright. The uppermost float included a downward-looking Acoustic Doppler Current Profiler

(ADCP, 75 Hz) for measuring current profiles (velocity and direction) and particle backscatter intensities, and a XEOS iridium beacon and flasher on top.

Table. 1. Layout of moorings' instruments as an example of sampling site M1

Instrument name	Description	Approx. water depth (m)
Benthos floats	Floats	720
Smartie float 500	Float with beacon + flasher + downward looking ADCP	750
SBE MicroCat CTD	CTD – Conductivity Temperature & Depth sensor	1190
Technicap PPS 5/2	Sediment trap with 24 bottles + tilt meter	1200
Smartie float	Float with 500kg buoyancy	1250
Aanderaa RCM	Current meter	3480
SBE MicroCat CTD	CTD – Conductivity Temperature & Depth sensor	3490
Technicap PPS 5/2	Sediment trap with 24 bottles + tilt meter	3500
Benthos floats	Floats to retrieve mooring	40m above bottom
Aanderaa RCM	Current meter	20m above bottom
Releasers	To detach mooring from anchor	10m above bottom
Anchor	Steel weight 2000kg	bottom

Generally, current velocities did not exceed 12 cm s^{-1}, which is considered a threshold for unbiased collection of settling particles (Knauer and Asper, 1989). Current-meter measurements showed that the average velocities around each mooring were < 6 cm s^{-1} in the deep and bottom ocean at around 3500 and 4600 m water depth, respectively and < 10 cm s^{-1} at around 1200 m water depth as measured by the ADCPs. For only a few days during

10 the entire sampling period current velocities exceeded the 12 cm s^{-1} for the upper sediment traps at 1200 m at the sites M2 and M3, while at M4 maximum velocities at 3350 m reached 19 cm s^{-1} in early August 2013. All other sensors showed that the sediment traps at sites M1 to M4 remained well within 5° from the vertical and at constant depths during the entire sampling period. Only during two periods at site M5 current velocities exceeded 12 cm s^{-1} to the extent of biasing collection efficiency: in February 2013 and late March 2013. This caused a downward

15 movement of the traps as recorded by increased pressure (depth) by both CTDs, as well as deviations of up to 14° and 12° from the vertical, respectively, as measured by the tilt meters, affecting three sample intervals at station M5 (intervals #8, 10 and 11). For these three intervals we adjusted the total mass flux using $F = F_t - (1+1.4\sin 2\theta)$ with F being the vertical flux, F_t the flux in the tilted trap, and θ the degree of tilt from the vertical (Gardner, 1985).

20 Each sediment trap has a collecting area of 1m^2 and is equipped with an automated rotary collector carrying 24 sampling cups. All traps collected the settling particles simultaneously and synchronously in 16-day intervals, starting on October 19, 2012 and ending on November 7, 2013. Prior to deployment in 2012, sampling cups had been filled with filtered seawater from the respective sampling depths at 1200 m and 3500 m, using HgCl$_2$ as a biocide (to an end concentration of 1.3 g/L) and Borax (Na$_2$[B$_4$O$_5$(OH)$_4$] *10H$_2$O; end concentration 1.3 g/L) as a

25 buffer at pH 8.5. Both additives increased the density to limit exchange with ambient seawater. Seven sediment traps were recovered successfully during RV Pelagia cruise 64PE378 in November 2013 (Stuut et al. 2013). These include three upper (1200 m) sediment traps at sites M1, M2 and M4 and four lower (3500 m) sediment traps at sites M2, M3, M4 and M5 (Fig. 1, Table. 2). On board, the pH of the supernatant solution was measured and an aliquot of supernatant liquid was analysed for nutrient concentration (SiO$_4^{4-}$, NH$_4^+$, PO$_4^{3-}$) for shipboard quality

30 control. When necessary, samples were post-poisoned and brought to an appropriate pH when lower than 8 to prevent CaCO$_3$ dissolution. Samples were kept dark and cool at 4^{0}C until further processing.

Table. 2. Sediment trap details. Sampling was performed simultaneously and synchronously from October 19, 2012 until November 7, 2013 (384 days). (mbsl = meter below sea level, MAR = Mid-Atlantic Ridge)

Trap	Position	Bottom depth (m)	Trap depth (mbsl)	Distance to African coast (km)	Closest horizontal distance to seafloor at trap depth (km)
M1U	12°00'N, 23°00'W	5000	1150	700	610
M2U	13°81'N, 37°82'W	4790	1235	2300	2260
M2L			3490		520 (MAR)
M3L	12°39'N, 38°63'W	4640	3540	2400	500 (MAR)
M4U	12°06'N, 49°19'W	4670	1130	3500	640
M4L			3370		580 (MAR)
M5L	12°02'N, 57°04'W	4400	3520	4400	63

3 Methods

The following paragraphs describe the different methods used to analyse particle fluxes and the element and biological composition of the specific samples. Due to the different nature and amount of material, i.e. the dry dust from the on-land dust collector in Iwik and the wet sediment trap samples from the deep ocean, not all methods were applicable to all samples. While for the marine sediments the total, biological and residual mass fluxes were determined, as well as their element composition, the Iwik samples were analysed exclusively for their total mass and horizontal dust flux at 290 cm as well as their element composition.

3.1 Particle Mass Fluxes

From the land-based dust collectors, all dust was removed from each sample bottle by loosening and shaking the dust out of the bottles. The removed dust was weighed on a micro-balance. Dust fluxes represent the horizontal transport fluxes of Saharan dust in the source. It is estimated by equation (1)

$$F_{MWAC} = \frac{MAR}{A} * \frac{1}{n} \tag{1}$$

where F is the dust flux (g m^{-2} d^{-1}), MAR is the mass accumulation rate (g d^{-1}), A is the cross-sectional area of the inlet tube of the MWAC sampler (m^2) and n is the estimated sampling efficiency of the MWAC bottles. The sampling efficiency of the MWAC samplers is between 75 % and 90 % for 30 µm dust (Goossens and Offer, 2000), which is within a similar size fraction of the Iwik dust (Friese et al. 2017).

For the vertical (downward) marine particle fluxes from the sediment traps, the samples were wet-sieved over a 1 mm mesh, wet-split in five aliquot subsamples using a rotary splitter (WSD-10, McLane Laboratories), washed to remove the HgCl$_2$ and salts, and centrifuged. Afterwards samples were freeze-dried and ground. Total mass fluxes refer to the < 1 mm size fraction and were determined by weighing two freeze dried 1/5 aliquots for every sample. Average weight differences between replicate aliquots were within 2.4% (SD = 2.2) and less than 12%, with 87% of all samples differing < 5% between splits. Total mass fluxes were determined by equation (2)

$$F = MAR * A^{-1} * d^{-1} \tag{2}$$

where F is the total mass flux (mg m^{-2} d^{-1}), MAR is the mass accumulation rate (mg), A is the sediment trap funnel opening (m^2), and d the sampling time interval.

Total nitrogen (TN), total carbon (TC) and organic carbon (TOC) content were determined with a Thermo Scientific Flash 2000 Elemental Analyser. Samples for TOC measurements were decalcified by acid fuming with a subsequent addition of 2 N HCl and dried in an oven at 60^0 C. Samples for TN and TC measurements remained untreated. Carbonates were calculated as $CaCO_3$ = (TC – TOC) * 8.33 and organic matter as OM = 2*TOC. The conversion factor for $CaCO_3$ $CaCO_3$ is based on its stoichiometry, given 100 mol/g of $CaCO_3$ for 12 mol/g of carbon, resulting in a factor of 100/12 = 8.33. The calculation factor for organic matter varies from 2.0 in the eastern Atlantic Ocean to 2.5 in upwelling areas (Fischer and Karakas, 2009;Jickells et al., 1998;Klaas and Archer, 2002;Thunell et al., 2007); due to poorly constrained composition of the actual organic matter. We chose to use the factor of 2 for better comparison to particle fluxes influenced by Saharan dust deposition off Cape Blanc (Fischer and Karakas, 2009;Fischer et al., 2007;Wefer and Fischer, 1993).

Biogenic silica (BSi) was analysed by sequential alkaline leaching on a HITACHI U-1100 spectrophotometer after Koning et al. (2002). A standard amount of 25 – 30 mg of ground sample was placed in a 0.5 M NaOH solution at 85° C, to dissolve the biogenic silica, which subsequently reacted with a sulphuric acid-molybdate solution to form a blue molybdate complex. The complex was prevented from molybdate reduction and stabilized by adding oxalic and ascorbic acid, respectively. The solution was flushed through a photocell where the absorption of the blue complex was measured at the defined 660 nm (Grasshoff et al. 1983) and recorded every second. Each sample was run for 60 to 90 minutes. Results were evaluated with a weekly measured standard calibration curve (R^2 > 0.99) and calculated with the MS Excel data solver tool, extrapolating the dissolution curve to time zero to correct for contribution of non-biogenic silica (DeMaster, 1981) The diatom reference material (pure *Thalassiosira punctigera* from the North Sea) is measured with a reproducibility of ±0.46 % and sample reproducibility is ±0.36%. For estimating mass fluxes, BSi is expressed as $BSiO_2$ (BSi*2.139), although this conversion systematically underestimates the actual mass by 10-20 % given the crystal water associated with the opaline silica of which the siliceous plankton consists (Mortlock and Froelich, 1989).

The remaining, residual mass fraction is often referred to as the lithogenic fraction (Fischer and Wefer, 1996;Wefer and Fischer, 1993;Fischer et al., 2016;Fischer and Karakas, 2009;Neuer et al., 2002) since it contains all the refractory lithogenic particles (quartz, clay minerals, feldspars). The residual mass is defined by subtracting the biogenic $CaCO_3$, $BSiO_2$ and OM from the total mass (Eq. 3) and includes all Saharan dust:

$$\text{Residual mass = Total mass} - CaCO_3 - BSiO_2 - OM \hspace{3cm} (3)$$

However, this residual fraction potentially also includes biogenic phosphates and sulphates, as well as particles of volcanogenic, cosmogenic and anthropogenic origin. In addition, crystal water associated with the opaline silica and the O-H content of organic matter and clay minerals also contribute to the residual mass. Therefore, the residual mass fraction is most likely overestimated while the marine biogenic fraction is underestimated.

3.2 XRF element analysis

The elemental composition of each sediment trap sample was determined by X-ray fluorescence (XRF) using the Avaatech XRF core scanner (Richter et al., 2006). This analytical technique has the important advantage that it is non-destructive, allowing that very small-size samples – such as sediment trap samples – can be used for other analyses after measurement. XRF scanning results in semi-quantitative compositional data (Richter et al., 2006), being expressed as intensities (i.e. counts or counts per second), which we normalize to the total counts to take

into account the closed sum of geochemical data. We analyse our data as normalized element intensities, using the advantage that XRF-scan measurements on homogenised dry sediment trap samples largely avoid physical properties biasing, e.g. wet down-core XRF measurements (Tjallingii et al., 2007;Weltje and Tjallingii, 2008). For dry-powder samples, Tjallingii et al. (2007) showed that element intensities are proportional to their chemical concentration, which we confirm by measuring 13 standards with various matrices, including marine sediments that have a similar matrix to sediment trap samples (Supplement S1).

Ground sediment trap samples (~25 mg) were pressed in polyethylene cylinders with a circular recess of 6 mm and 1.5 mm depth and covered with SPEXCerti Ultralene® foil. All samples were measured with a 4x4 mm slit size at a voltage of 10, 30 and 50 kV (elements: Al, Si, K, Ca, Ti, Cr, Mn, Fe, Cu, Zn, Sr, Zr and Ba), with an electric current of 1.5, 1.3 and 0.8 mA and a measurement time of 20, 40 and 80 seconds, respectively. All measurements were performed five times, and average values for these measurements are shown. The elements Ti, Al, Fe and K were chosen and shown, since they are only present as main or minor elements in lithogenic minerals like clays, quartz, and feldspars, rather than in any biogenic mineral formed in the ocean, while Si represents both lithogenic Si minerals (clays, quartz, and feldspars) but also biogenic produced silica ($BSiO_2$), as found in phytoplankton diatoms or zooplankton radiolarians. Pearson correlation was applied to the whole dataset of which we show the five elements Ti, Al, Fe, Si and K in table S2. Five of the sediment trap samples (M1U #9, 12 and 24; M4U #12 and 24) could not be analysed due to insufficient material.

Two certified external standards (powdered marine sediment MESS-3 and PACS2) were used for quality control of the XRF measurements (Supplement S1), and were both analysed within each run of ~25 samples in exactly the same way as the sediment trap samples. These standards showed a precision, expressed as relative standard deviation (RSD = standard deviation / average of replicates x 100%), < 7 % for all normalized element intensities. Moreover, the normalized intensities of these two standards closely follow the calibration line of all 13 standards (Supplement S1).

4   Results

Horizontal transport fluxes from the land-based MWAC sampler are given in g m^{-2} d^{-1}. The vertical (downward) deposition fluxes from seven sediment traps deployed across the Atlantic Ocean are treated in downwind succession from east to west, starting at ocean site M1 closest to Africa, to ocean site M5 closest to the Caribbean. For each trap, the relative contribution of the biogenic components $CaCO_3$, $BSiO_2$, OM, and the residual mass fraction are given, in addition to the total mass flux, the flux of each biogenic component and that of the residual mass fraction, expressed both in mg m^{-2} d^{-1} and g m^{-2} a^{-1}. The biogenic components are produced by autotrophic phytoplankton and heterotrophic zooplankton. In particular, phytoplankton $CaCO_3$ producers are mainly coccolithophores while zooplankton $CaCO_3$ is mainly from foraminifera and gastropod shells. The $BSiO_2$ is primarily produced by the phytoplankton diatoms and zooplankton radiolarians. Seasonal variations are shown for specific fluxes as deviation from their annual mean, together with the grain-size distribution of Saharan dust (Van der Does et al. 2016) for the residual mass fraction in the same material. To evaluate the residual mass fraction in the sediment traps, we compare XRF data from MWAC samplers with those from the sediment traps. The horizontal mass fluxes of the land-based dust collectors in Iwik are almost 100 % pure dust with negligible contribution of organic matter and fresh water diatoms from paleolakes and can therefore be used for chemical element comparison to the residual mass fraction from the sediment traps. Deviations between the chemical composition of the MWAC samplers and the sediment traps reveal compositional changes.

4.1 Horizontal land-based transport fluxes at Iwik

The total mass fluxes of the MWAC samples at 290 cm height show significant month-to-month differences (Fig. 2). Highest dust fluxes of around 360 and 230 g m^{-2} d^{-1} were found during spring in April 2013 and during summer in August 2013, respectively. Local wind speeds at 10 m above the displacement height (MERRA model, NASA GES DISC) show monthly average velocities between 3 and 7 m s^{-1} with higher wind speeds in early summer and lower wind speeds in fall. Throughout the entire sampling period, the wind speeds are above desert pavement threshold velocities of 1.5 to 3 m s^{-1} (Pye, 1987), suggesting also dust contribution from adjoining areas.
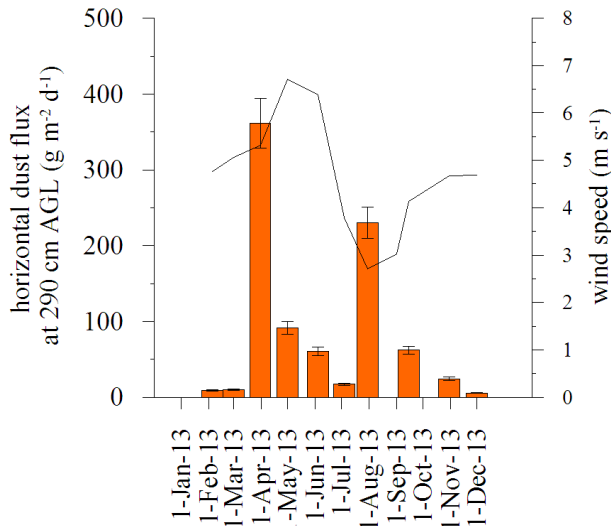
Figure. 2. Horizontal transport fluxes of Saharan dust from the land-based MWAC sampler in Iwik, Mauretania (19° N, 16° W) between January and December 2013 in orange bars. Error bars show the MWAC sampler efficiency of 75 to 90 %. Monthly averaged wind speed at 10 m above displacement height (MERRA model) around the Iwik location is indicated as a black line (data obtained from the Giovanni online data system, NASA GES DISC). AGL = above ground level

4.2 Mass fluxes at ocean site M1

The shallow sediment trap at 1150 m water depth at site M1 collected a fairly steady total mass flux year round (Fig. 3) with a daily average of approximately 100 mg m^{-2} d^{-1} which equals an annual export of 40.7 g m^{-2} a^{-1} (Table 3). The mass fluxes of the marine biogenic constituents (CaCO$_3$, BSiO$_2$ and OM) follow those of the total mass and are in close relation to each other. The composition of the trapped material is dominated by CaCO$_3$ (21-45 %) and the residual mass fraction (30-58 %), with minor OM (14 %) and BSiO$_2$ (10 %). A clear seasonal pattern in the total mass flux is absent, although a peak flux is recorded in March (interval #9). Relative to the annual mean, biogenic matter fluxes are high during winter and spring and low during fall and especially summer (Fig. 4). Consequently, the residual mass fraction shows the opposite, with a low relative abundance in winter and spring and a high in summer and fall. The variation of the residual mass flux is consistent with the long-term seasonal transport of Saharan dust above the eastern tropical North Atlantic (Chiapello and Moulin, 2002). The residual mass flux ranges from 32-71 mg m^{-2} d^{-1} with an average of 47.7 mg m^{-2} d^{-1} (17.4 g m^{-2} a^{-1}) and slightly elevated values during summer and fall (#16, 18, 19 and 22) but with a peak in March (#9). A pronounced seasonality is also seen in the grain-size distributions of the same material with coarser grained Saharan dust in summer and finer grained dust in winter (Van der Does et al. 2016).

4.3 Mass fluxes at ocean site M2

Total mass fluxes at site M2 average 40 mg m^{-2} d^{-1} (14.4 g m^{-2} a^{-1}) in the upper trap at 1235 m and 55 mg m^{-2} d^{-1} (19.9 g m^{-2} a^{-1}) in the lower trap at 3490 m (Fig. 3, Table 3). Peak fluxes are recorded in March and late April (intervals #9 and 12). The composition of the material is rather similar in the upper and lower trap. In general, the trapped material is dominated by CaCO$_3$ (56 % and 59 %, respectively), followed by the residual fraction (27 % and 28 %, respectively), OM (11 % and 7 %, respectively) and BSiO$_2$ (both about 6 %). No clear seasonal pattern is seen in either traps in the total mass fluxes despite some peaks occur in the upper and the lower trap during the same sampling intervals (Fig. 4). No clear seasonal pattern appears in the biogenic fractions, although CaCO$_3$ and BSiO$_2$ tend to be relatively enhanced during spring and summer, and OM in fall. Therefore, the resulting residual fraction is relatively enriched during summer and fall and suppressed during winter and spring. The small contribution of the residual fraction in spring is also expressed in its mass flux, yet is more variable in the upper trap than in the lower trap. It ranges between 4-32 mg m^{-2} d^{-1} with an average of 10.6 mg m^{-2} d^{-1} (3.9 g m^{-2} a^{-1}) in the upper trap and varies between 10-22 mg m^{-2} d^{-1} with an average of 15.3 mg m^{-2} d^{-1} (5.6 g m^{-2} a^{-1}) in the lower trap. This also holds for the grain-size distributions, while the dust particles in the upper trap show a distinct seasonality with coarser grains in summer and fall, the grain sizes of the dust particles in the lower trap fluctuate with no clear seasonality (Van der Does et al. 2016).

4.4 Mass fluxes at ocean site M3

At site M3 about 220 km south of site M2, the total mass flux at 3540 m water depth amounts to 70 mg m^{-2} d^{-1} (14.4 g m^{-2} a^{-1}) (Table 3). A double peak flux occurs during summer (intervals #15 &16). The peak fluxes are mainly CaCO$_3$, which forms more than half of the total mass (52 %) followed by OM (8 %) and BSiO$_2$ (7 %). Around one third (33 %) of the total mass resides in the residual fraction, with maxima during fall and minima during spring. Although the seasonality is weak small peaks appear, especially in June (Fig. 3). The residual mass fraction varies between 13-38 mg m^{-2} d^{-1} with an average of 23.0 mg m^{-2} d^{-1} (8.4 g m^{-2} a^{-1}). The differences from the mean contribution of the biogenic components show enhanced CaCO$_3$ in winter and spring and BSiO$_2$ in summer and fall 2013 (Fig. 4). The OM shows little seasonal variation, albeit slightly suppressed during spring.

4.5 Mass fluxes at ocean site M4

Average total mass flux amounts to 85 mg m^{-2} d^{-1} (30.9 g m^{-2} a^{-1}) in the upper trap and 64 mg m^{-2} d^{-1} (23.2 g m^{-2} a^{-1}) in the lower trap (Table 3). Both traps intercepted two striking peak flux events, the first during spring (late April) and the second during fall 2013 (late October/early November), when total mass fluxes exceeded 200 mg m^{-2} d^{-1} in the upper and 100 mg m^{-2} d^{-1} in the lower trap (Fig. 3). The peak fluxes differ in composition: while the peak in spring is CaCO$_3$ dominated (60 % in the upper trap and 73 % in the lower trap), the peak in fall is marked by BSiO$_2$ (25 % and 28 % in the upper and the lower trap, respectively). In addition, both peaks show elevated OM fluxes in both traps. Residual fluxes are elevated in the upper trap for the peak fluxes as well, but in the lower trap only in fall. Overall, the residual mass fraction ranges between 14-87 mg m^{-2} d^{-1} with an average of 24.0 mg m^{-2} d^{-1} (8.7 g m^{-2} a^{-1}) in the upper trap and varies between 8-42 mg m^{-2} d^{-1} with an average of 17.4 mg m^{-2} d^{-1} (6.4 g m^{-2} a^{-1}) in the lower trap. The seasonal variability of the grain-size distributions become smaller but are still visible in the upper trap with coarser grained dust during summer and fall (Van der Does et al. 2016). Seasonal variability of BSiO$_2$ is dominated by the exceptionally high peak in fall (Fig. 4).

4.6 Mass fluxes at ocean site M5

The sediment trap at 3520 m water depth at the western most ocean site M5 intercepted an average total mass flux of 116 mg m^{-2} d^{-1}, which equals an annual mass flux of 42.2 g m^{-2} a^{-1} (Fig. 3, Table 3)). Most of the trapped material resides in the residual mass fraction (45 %), followed by CaCO$_3$ (33 %), BSiO$_2$ (17 %) and OM (6 %). Seasonal variability is clear in the total mass flux with maxima during spring and halfway through summer, followed by a changeover in August to lower values during the second half of summer and fall 2013 (Fig. 4). Clearest seasonality is shown by BSiO$_2$ with a pronounced maximum in summer to late fall and minima in winter and spring. Seasonality is less clear in CaCO$_3$ and absent in OM, while the residual mass shows maxima in spring and minima in summer to late fall. It ranges between 17-125 mg m^{-2} d^{-1} with an average of 52.3 mg m^{-2} d^{-1} (19.1 g m^{-2} a^{-1})The grain sizes of the residual fraction become smallest at this western most station and varies around the clay size fraction (Van der Does et al. 2016).

Table 3. Yearly mass fluxes of measured flux parameters.

Trap	Total Mass Flux	CaCO$_3$	BSiO$_2$	OM	Residual mass	CaCO$_3$	BSiO$_2$	OM	Residual mass
	mg m^{-2} d^{-1} (g m-2 a-1)	%				mg m^{-2} d^{-1} (g m^{-2} a^{-1})			
M1 U	111.6 (40.7)	33.9	9.7	13.6	42.7	37.8 (13.8)	10.9 (4.0)	15.2 (5.6)	47.7 (17.40)
M2 U	39.5 (14.4)	56.0	5.9	11.3	26.8	22.2 (8.1)	2.3 (0.8)	4.5 (1.6)	10.6 (3.9)
M2 L	54.6 (19.9)	59.2	5.7	7.2	27.9	32.3 (11.8)	3.1 (1.1)	3.9 (1.4)	15.3 (5.6)
M3 L	70.4 (25.7)	52.0	6.9	8.4	32.7	36.6 (13.4)	4.9 (1.8)	5.9 (2.2)	23.0 (8.4)
M4 U	84.8 (30.9)	48.3	10.8	12.6	28.3	41.0 (14.7)	9.2 (3.4)	10.7 (3.9)	24.0 (8.7)
M4 L	63.6 (23.2)	53.0	10.7	8.9	27.4	33.7 (12.3)	6.8 (2.5)	5.7 (2.1)	17.4 (6.4)
M5 L	115.6 (42.2)	32.5	16.5	5.7	45.3	37.6 (13.7)	19.1 (6.7)	6.6 (2.4)	52.3 (19.1)
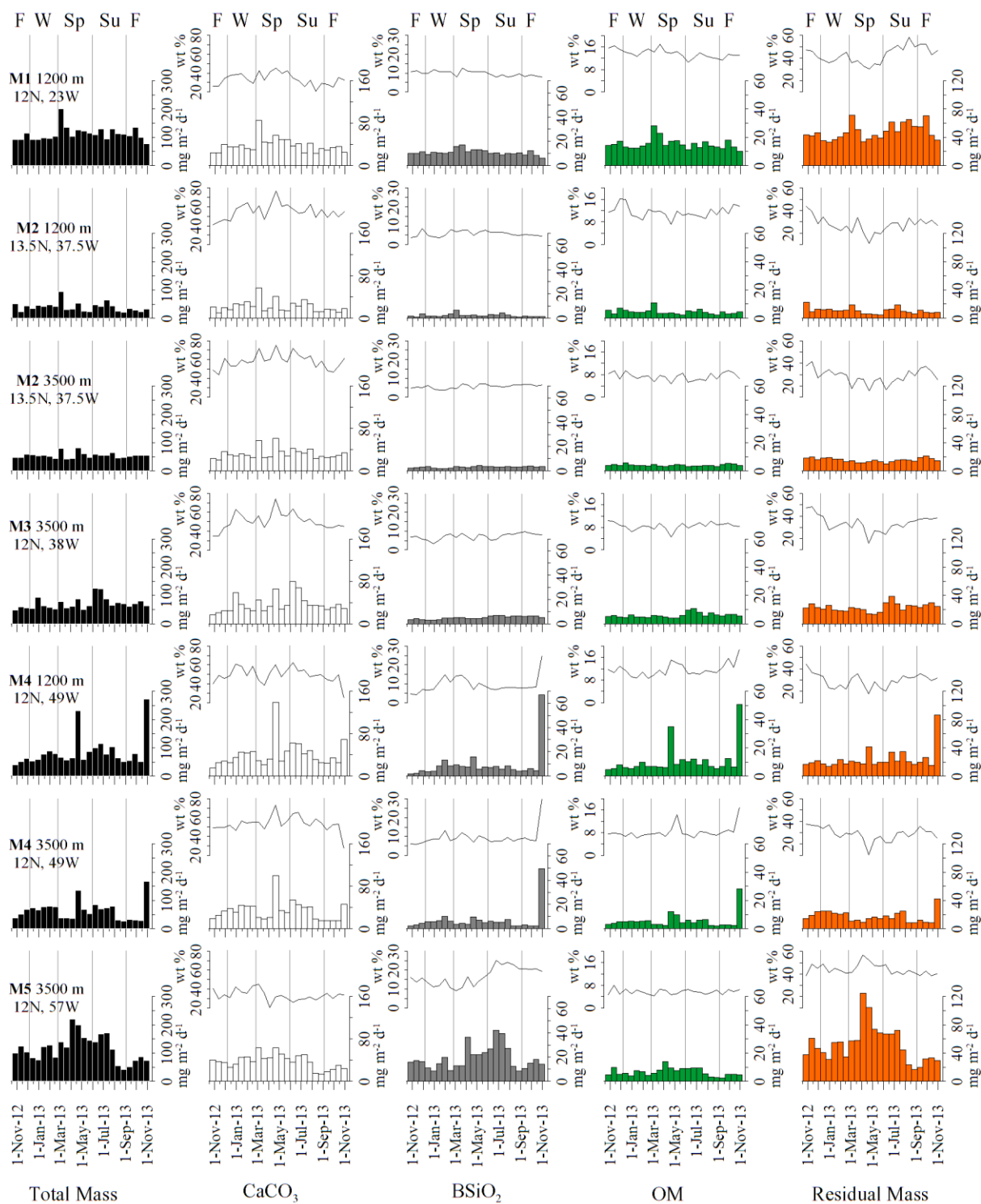
Figure 3. Mass fluxes at ocean site M1U to M5L in mg m^{-2} d^{-1} (bars) for total mass (black), CaCO$_3$ (white), BSiO$_2$ (grey), organic matter (green) and the residual mass fraction (orange); black lines represent their relative contributions (wt%). F = Fall, W = Winter, Sp = Spring, and Su = Summer.
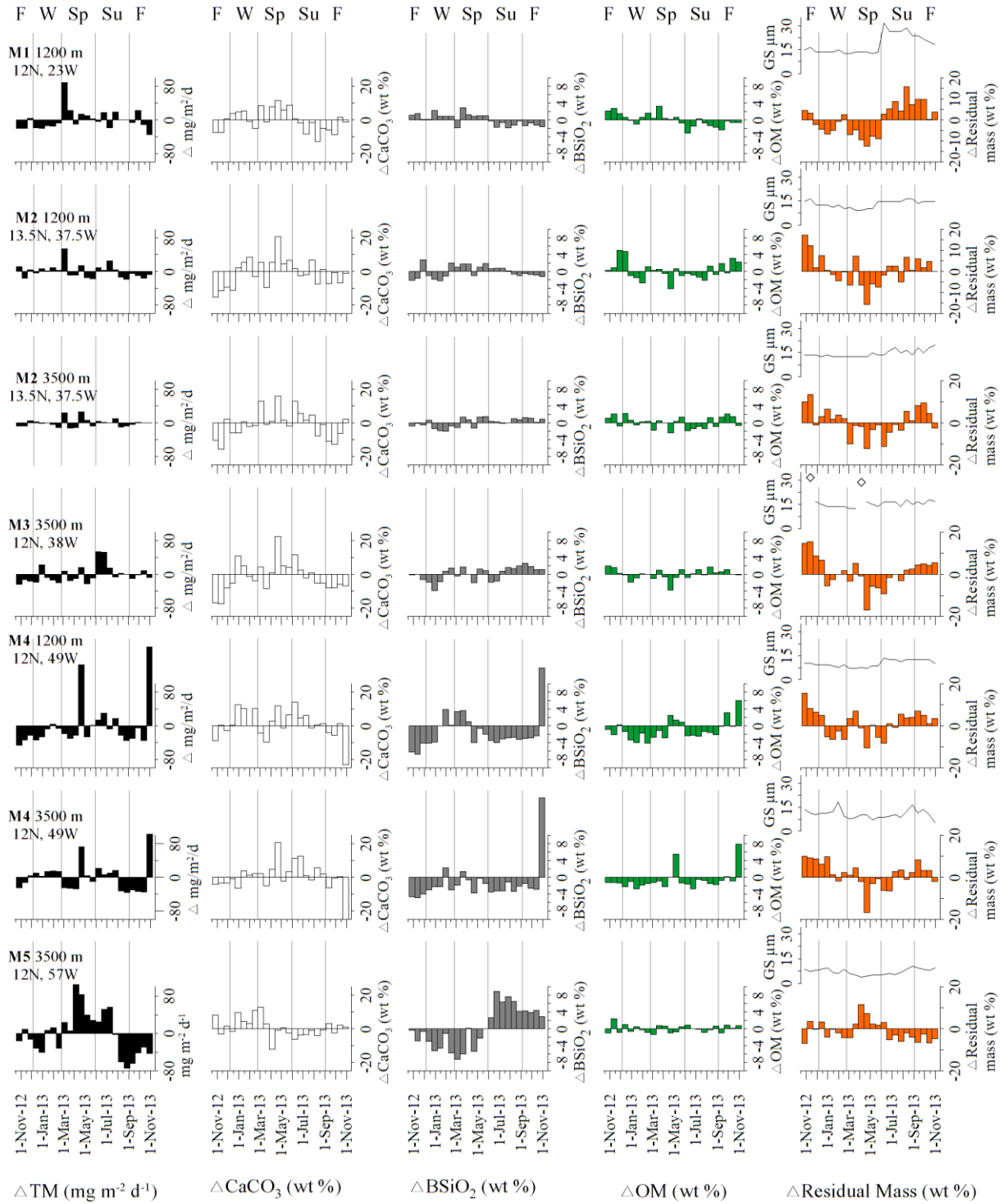
Figure 4. Deviation from the flux-weighted annual mean for total mass (black), CaCO3 (white), BSiO2 (grey), organic matter (green) and the residual mass fraction (orange) at ocean sites M1U to M5L. Black line represents modal grain sizes of Saharan dust of the same sample, diamonds in M3 are outliers (data Van der Does et al. 2016). F = Fall, W = Winter, Sp = Spring, and Su = Summer.

4.7 Molar C : N ratios

Total organic carbon (TOC) and nitrogen (TN) are highly correlated at both trap depths (Fig. 5). The upper traps of the moorings M1, M2 and M4 show higher TOC and TN contents than the lower traps of the moorings M2, M3, M4 and M5. However, two fluxes (interval #13 and 24) at site M4L contain as much TOC and TN as found in the upper traps. The molar C : N ratio of all traps is on average 9.17 with a standard deviation of 0.95. Overall, the ratios in the lower traps are slightly higher than in the upper traps, but without significant changes. The highest value (10.26) is reached at site M3L and the most uniform ratios between 8.46 and 9.65 are observed at ocean site M1U. The molar C : N ratios are in the typical range of sinking detritus collected in deep sediment traps and are comparable to the material collected off Mauritania but without seasonal differences (Fischer et al. 2016).
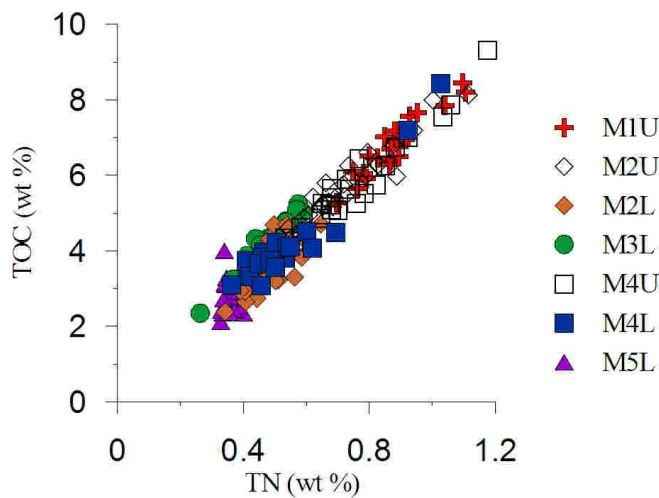
Fig. 5. Total organic carbon (TOC) versus total nitrogen (TN) content for all ocean sites M1-M5.

4.8 XRF element ratios

We identify the residual mass fraction as lithogenic fraction by elements such as titanium (Ti), aluminium (Al), iron (Fe) and potassium (K). These elements are incorporated in mineral dust, in especially in aluminosilicates and feldspar, oxides and hydroxides and are incorporated in crystal lattice (Scheuvens et al., 2013). Although K is also detected in biomass burning aerosols (Cachier et al., 1995), the high correlations between K and the other lithogenic elements show that the contribution of biomass burning K is minor in our samples. Normalized intensities of the lithogenic elements are highly correlated with the residual mass fraction and are therefore thought to represent the deposition flux of Saharan dust (Fig. 6). However, spatial differences from east to west indicate the continuous enrichment of especially Al and Fe from M1 to M5, and to an offset of higher K at M5, while Ti stays constant. The modal particle sizes of the dust (Van der Does et al. 2016) do not show a relation to the lithogenic elements. Best relations found were in the west at site M5 where sizes and lithogenic elements are negatively correlated (Al, $R^2=0.54$ and K, $R^2=0.44$).

Normalized intensities of Al and Ti are highly correlated as well, both within the time series in Iwik and throughout all seven sediment traps deployed in the deep ocean (Fig. 7; Table S2, S3). The dust sample from Iwik and the samples at the proximal ocean site M1 are most similar in element composition, having the same slope and intercept for Ti and Al normalized intensities (Table S3). Further downwind, Ti/Al intensity ratios are lower but very similar at M2, M3 and M4U, while those at M4L and M5L have very similar but lower slopes (Fig. 7).
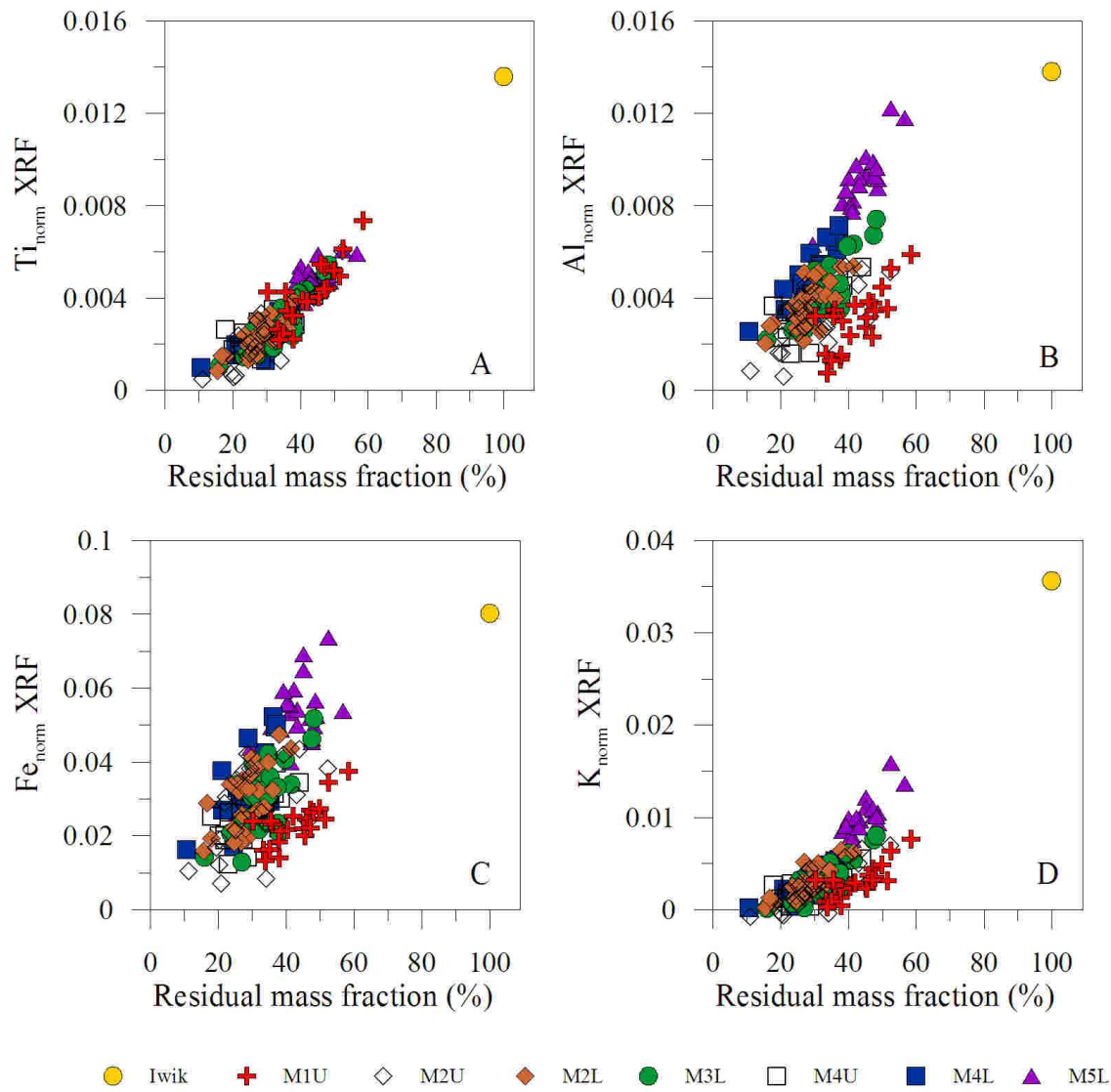
Fig. 6. Comparison of the lithogenic elements Ti (A), Al (B), Fe (C) and K (D) normalized to total XRF counts versus the residual mass fraction in all sediment traps and the average of the land-based dust collectors in Iwik.
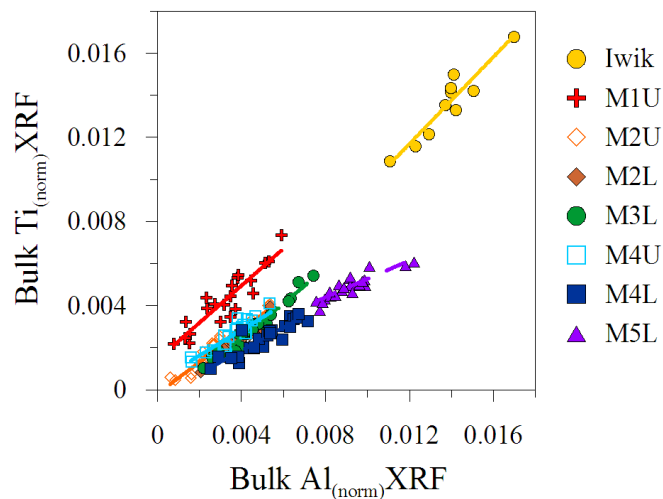
Fig 7. Comparison of bulk Ti and Al, normalised to total XRF counts for all seven sediment traps and the on-land dust collectors in Iwik, Mauritania.

Saharan dust mostly consists of lithogenic silicates such as quartz, clay minerals and feldspars (Caquineau et al., 2002) that contribute to the total silica content in addition to the biogenic silica found in the sediment traps derived from skeletal plankton such as diatoms and radiolarian. Regression of biogenic silica determined by sequential

5   leaching to the total silica determined by powder XRF show a clear downwind increase from M1 to M5 (Fig. 8). Starting at ocean site M1, closest to the Saharan dust source, correlation is weakly negative, then vanishes at M2 and becomes positive and progressively stronger from M3 to M5.
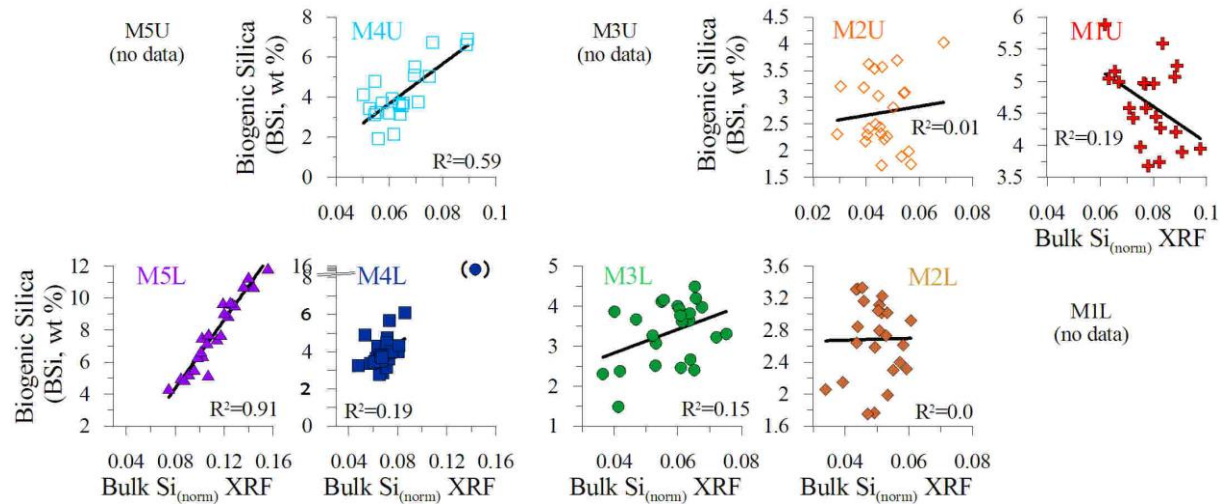
Fig 8. Biogenic silica versus total silica in particulate fluxes at five sites across the North Atlantic with
10   **sampling site M1 in the east (right) and M5 in the west (left).**

5   Discussion

We provide the first comprehensive time series of biogenic particle fluxes and Saharan dust deposition from source to sink across the equatorial North Atlantic Ocean. The land-based dust collectors in Iwik are located in the coastal region of western Mauritania, in potential source area 2 (PSA 2), which is one of the major source areas of dust

15   that is transported across the Atlantic Ocean to the Americas (Scheuvens et al., 2013). The transport fluxes are highest in spring and summer (Fig. 2). The spring high can be related to the trade-wind intensities at lower altitudes, whereas the summer high point to sporadic dust storms, invisible on land by satellites. Backward trajectories reveal that the location in Iwik is a transit area for long-range transported Saharan dust (Friese et al. 2017). Overall, the horizontal Saharan dust flux from the land-based MWAC samplers in Iwik cannot be compared directly to the

20   downward flux in residual mass to in the sediment traps. However, they are compositionally the same, especially at the ocean site M1 as indicated by their similar Ti-Al slopes (Fig. 7). From site M1 we observe an overall decrease in both the residual mass and the marine biogenic matter fluxes westward to M2/M3 and M4. The much higher counts of lithogenic elements Ti, Al, Fe and K found in the dust at Iwik result from the absence of dilution by biogenic matter produced in the marine realm. While the Ti-Al slopes are the same at Iwik and ocean sites M1

25   through M4U, and Al, Fe and K counts are most similar at Iwik and M1 as well, but become significantly higher towards the west (Fig. 6), it suggests a downwind change in mineralogical composition of Saharan dust. At ocean sites M4L and M5L, both the Ti/Al slope is lower and the Al counts are higher especially at M5, indicating that a second source in addition to Saharan dust is involved, which may be derived from admixture of re-suspended clay-sized sediments advected towards the deep sediment traps. This is especially indicated by the offset of K at M5L.

30   Overall, we observe a downwind increase in the Al and Fe content of the residual mass fraction, which suggests an increase in clay minerals relative to quartz. A similar change in mineralogy was observed by Glaccum and

Prospero (1980) who compared the mineralogy at the eastern and western Atlantic Islands. Our observation is also supported by the clear downwind trend in the correlation between biogenic silica, as determined by sequential alkaline leaching, and total silica measured by XRF (Fig. 8). Such a downwind decrease in the relative amount of quartz may result from the increase of finer particles due to their slower settling speed, and a relative increase in platy clay minerals such as micas suspended in the atmosphere that can be transported over greater distances. This is consistent with the downwind decrease in grain size as observed by Van der Does et al (2016) on the same material.

5.1 Comparison with satellite observations

Saharan dust needs about a week (5 – 6 days) to cross the Atlantic Ocean from east to west as observed in satellite images (Prospero et al. 1970, 2014). Since the sampling interval of all sediment traps is 16 days, it is difficult to identify individual dust outbreaks as individual peaks in mass fluxes that decrease in amplitude from east to west. However, this seems to be the case for the peak fluxes occurring in summer, when there is an enhanced contribution by the residual fraction, especially closest to the African coast at the ocean site M1. Such enhanced fluxes in residual mass are found in intervals #16, #18 and #19 at site M1U, and M4U and #16 of M3L, corresponding to the period from 16 June to 2 July, from 18 July to 3 August, and 3 August to 19 August 2013, respectively. During these summer intervals, dust outbreaks leave the African coast at high altitudes and propagates westwards across the Atlantic (Fig. 9). Despite this apparently good correspondence between the satellite data and the sediment trap record, there are also other cases where the sediment traps did not seem to record specific dust outbreaks observed in satellite images. This may relate to the altitude at which the dust is travelling; in summer, dust travels through the high atmosphere, as opposed to winter-dust that travels in the low-level trade-wind zone. The diffuse cloud that is observed across a relatively wide band throughout the atmosphere in summer is interpreted from nadir-looking satellites as higher aerosol optical thickness than the relatively narrow and dense dust cloud that crosses the atmosphere in winter. Conversely, some sediment trap intervals recorded a residual mass peak in spring, e. g. interval #9 which could be followed in M1U, M2U, and M3L, (Fig. 3), when no evidence is found for the occurrence of dust events during that period (24 February – 12 March 2013) in satellite imagery. This could be reflecting the timing of satellite overpasses, which could potentially lead to missing short-term events. However, most dust events that are recorded by satellite images are visible as multiple-day events. The presence of clouds in virtually all satellite images is likely to at least partially obscure low-level winter dust outbreaks. Although satellite products are a great help to follow huge dust outbreaks crossing the Atlantic, our results illustrate that there is still a high degree of difficulty in matching specific dust outbreaks observed by satellites and the fluxes we measure in the deep sediment traps. This may also be enhanced by time lag between the deposition of Saharan dust on the ocean surface and their arrival at depth.
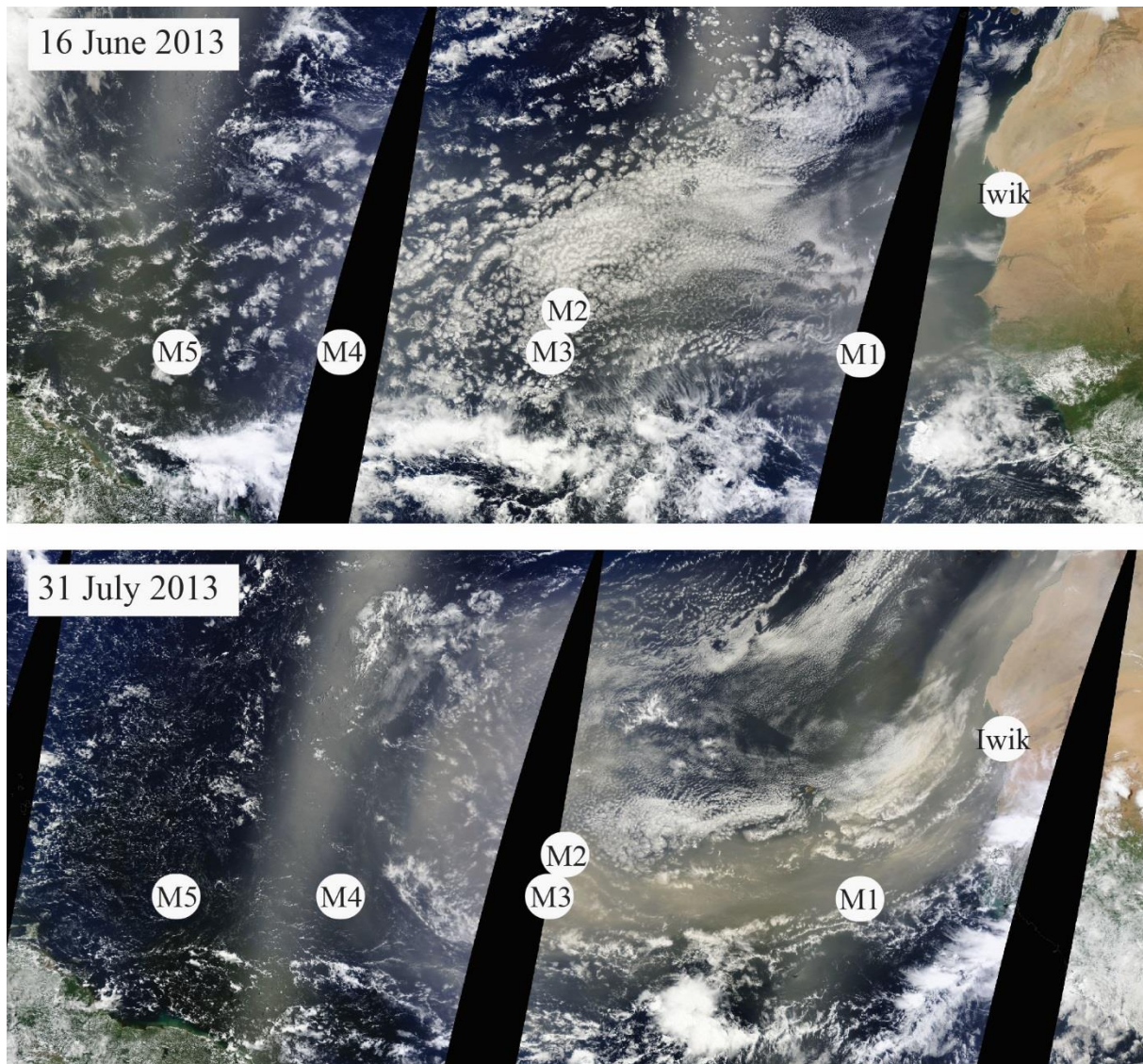
Fig 9. Satellite images (Images from NASA Worldview, MODIS Terra satellite) showing dust outbreaks propagating westwards from the African coast across the Atlantic Ocean, the location of the land-based dust samplers at Iwik and the five ocean moorings M1 through M5.

5.2 Gravitational settling and downward transport

Saharan dust deposited on the surface ocean is generally too fine to settle out as individual particles, except perhaps for larger and massive quartz particles. Rather, they remain effectively suspended until incorporated by organic matter aggregates such as "marine snow" and fecal pellets that accelerate settling to velocities in the order of 200 m d^{-1} (Knappertsbusch and Brummer, 1995;Berelson, 2002;Fischer and Karakas, 2009). Indeed, at site M4, both the traps at 1200 m and 3500 m intercepted two peak fluxes during the same 16-day interval, one in April and one in October (Fig. 3). Since these traps are 2300 m apart, this results in a settling velocity of at least 140 m d^{-1}. Higher settling velocities are conceivable for the fall peak fluxes at station M4, since the TOC and TN content (Fig. 5) of this peak flux in the lower trap is equally high as in all the upper traps (M1, M2 and M4), indicating rapid settling and little degradation. The same is observed at ocean site M2 for the flux peaks in March and in May (Fig. 3). However, the settling pathway might be different, as indicated by the higher total mass fluxes in the lower trap than the upper trap at site M2. Over the 2300 m distance of the upper and lower trap, the sinking particles are potentially subject to a variety of processes including remineralisation, disaggregation, or repacking, as well as horizontal movement of the particles, resulting in a greater catchment area (Waniek et al. 2000). Therefore, the

enrichment in the lower trap at site M2 might result from the greater catchment area of the deeper trap (Siegel and Deuser, 1997;Waniek et al., 2000). The same holds for the residual mass, which is more enriched in the lower trap compared to the upper trap. Consequently, time lags between Saharan dust outbreaks and transport in the higher atmosphere as observed in satellite images and their arrival in the upper sediment traps are at least a week and might take another path until arrival in the lower trap two weeks later. In this respect, buoys deployed now for time-series sampling of atmospheric dust just above the ocean surface at the same sites will serve as an intermediate between satellite observations of dust outbreaks and the actual deposition of dust on the surface ocean, which can be then followed down by the fluxes in the ocean.

5.3 Comparison with deep ocean mass fluxes off northwest Africa

The mass fluxes that we observe in the traps along the transect are in line with observations from sediment traps further north, off Cape Blanc on the Mauritanian continental slope at ~21°N, 20°W. For that site, Fischer et al., (2016) report total mass fluxes of 40.23 g m^{-2} per year averaged over a period of 25 years with much interannual but little seasonal variability. This compares well with our sampling site M1, where we measured a total mass flux of 40.7 g m^{-2} a^{-1}. Cape Blanc residual mass fluxes vary about 5 to 26 g m^{-2} a^{-1} (Fischer et al., 2016), which agrees very well with the average residual flux at site M1 of 17.4 g m^{-2} a^{-1}. At both sites the residual mass fluxes make up about a third of the total mass flux and up to 50% during dust events (Nowald et al., 2015). Biogenic mass fluxes in the Cape Blanc area are generally also high, also owing to the upwelling of cold, nutrient-rich waters that cause high primary productivity in the surface waters. However, biogenic mass fluxes are about the same as found at M1, where no upwelling-stimulated productivity occurs. At site M1 all biogenic particle fluxes are highest in comparison to the other sampling sites. The only exception is the BSiO$_2$ at site M5, which is by far the highest contribution of BSiO$_2$. The low flux of biogenic particles in the mid-Atlantic Ocean (M2 to M4) reflect the limited availability of nutrients and low productivity in the oligotrophic ocean. The higher biogenic mass fluxes closest to either continent (M1 & M5) may have been enhanced by the higher lithogenic input, especially from higher Saharan dust input at site M1, as mineral dust enhances the settling of organic matter through the water column (Ittekkot et al., 1992;Hamm, 2002)

Moreover, mass fluxes collected by sediment traps off Cape Blanc, for example, are affected by lateral input from re-suspended sediments that are advected from the Mauritanian continental slope in nepheloid or bottom layers (Fischer et al., 2009). Similar lateral transport of resuspended sediments (Van Raaphorst et al., 2001;Bonnin et al., 2006) may also have come from the nearby Barbados continental slope and contributed to the high fluxes of the residual mass fraction at ocean site M5 (Fig. 3), which is relatively close to the Barbados margin, around 63 km to the trap depth at 3500 m (Fig. 1B, Table 2). This admixture of resuspended sediments is also suggested by the lower Ti/Al ratios and high K contents at M5, and to a far lesser extent also in the deep trap at M4 although residual mass fluxes at this site are significantly lower (Fig. 3). The enrichment in Al, Fe and K indicates the addition of Al-Fe-K-rich clay minerals from a second source next to the Saharan dust deposited at these sites. This second source of sediments in the deep traps potentially also causes the negative correlation between the residual masses at M5 and M1, while those between M1 to M4 are all positively correlated (Table S4). Nevertheless, the particle-size distributions at M4 and M5 (Van der Does et al. 2016) alone do fit the general pattern of decreasing particle size with increasing distance from the Saharan dust source, not expecting fluvial input from the west.

The particle fluxes at ocean site M5 deviate from the general pattern in terms of enhanced total and residual mass fluxes and seasonal biogenic-silica contribution. Due to its westernmost position, the deep sediment trap may have received considerable amounts of lithogenic or biogenic material originating from either the Amazon- or Orinoco

River, or both. The freshwater Amazon outflow disperses kilometres from the river mouth and affects the oceans' biogeochemistry (Yeung et al., 2012). Due to nutrient input, the occurrence of diatom-diazotroph associations is stimulated (Subramaniam et al., 2008). The fact that the biogenic silica correlates perfectly with the bulk silica (Fig. 8) possibly relates to the appearance of diatom phytoplankton and less contribution of quartz minerals.

6 Conclusions

The first-year results of our monitoring experiment yield valuable insights into the transport and deposition fluxes of Saharan dust between the African continent and the Americas. We demonstrate that the lithogenic particles collected in the sediment traps are similar to the dust collected on the African coast. With increasing distance from the source, lithogenic elements associated with clay minerals become more important relative to quartz settling out closer to the source. The total silica analyses show that the contribution by biogenic silica, produced by marine biota, increases significantly from east to west to the extent that virtually all silica consists of biogenic silica and lithogenic quartz is minor in the west furthest away from the African source(s). At the westernmost ocean site, enhanced residual mass fluxes collected by the deep sediment trap suggest admixing with a second source from resuspended ocean floor sediments. Tracing back individual dust outbreaks from satellite images to the arrival in the deep ocean sediment traps is still demanding given sampling resolution and the time lags involved. Best accordance of satellite images and the residual mass fraction was found for summer. The relative contribution of the residual mass fraction is found to be highly co-variant with typically lithogenic elements such as Al and Ti from Saharan mineral dust. While the temporal and spatial variability in residual mass fluxes corresponds to the changing chemical composition of Saharan mineral dust, they seem to overestimate the net fluxes due to underestimation of marine biogenic matter. To better approximate the deposition of Saharan dust, buoys that were deployed in 2013 should give information on precise fluxes, which can then be followed in the underlying sediment traps.

7 Data availability

Supplementary data are available at https://doi.pangaea.de/10.1594/PANGAEA.872093.

Acknowledgements

The Project is funded by ERC (project no. 311152) and NWO (project no. 822.01.008). We thank the crew of Meteor Cruise M89, Pelagia Cruise 64PE378 and NIOZ technicians for their contributions. Camara from the Parc National de Banc d'Arguin (PNBA) is thanked for assistance with the dust sampling in Iwik, Mauritania. Jort Ossebaar is thanked for helping with the EA analysis and Sharyn Ossebaar for assisting with the biogenic silica measurements. XRF-analysis was supported through the SCAN2 program (NWO project no. 834.11.003) and assistance by Rineke Gieles. Furu Mienis is thanked for helping with interpreting the current-meter data and assistance in the sediment-trap lab. The authors also acknowledge the MODIS mission scientists and associated NASA personnel for the production of the data used in this research effort. We thank three anonymous reviewers for their helpful contribution.

References

Armstrong, R. A., Peterson, M. L., Lee, C., and Wakeham, S. G.: Settling velocity spectra and the ballast ratio hypothesis, Deep Sea Research Part II: Topical Studies in Oceanography, 56, 1470-1478, http://dx.doi.org/10.1016/j.dsr2.2008.11.032, 2009.

Baker, A. R., Kelly, S. D., Biswas, K. F., Witt, M., and Jickells, T. D.: Atmospheric deposition of nutrients to the Atlantic Ocean, Geophysical Research Letters, 30, n/a-n/a, 10.1029/2003GL018518, 2003.

Berelson, W. M.: Particle settling rates increase with depth in the ocean, Deep-Sea Research Part II, 49, 237-251, 2002.

10   Bloemsma, M., Zabel, M., Stuut, J., Tjallingii, R., Collins, J., and Weltje, G. J.: Modelling the joint variability of grain size and chemical composition in sediments, Sedimentary Geology, 280, 135-148, 2012.

Bonnin, J., Van Haren, H., Hosegood, P., and Brummer, G.-J. A.: Burst resuspension of seabed material at the foot of the continental slope in the Rockall Channel, Marine Geology, 226, 167-184, http://dx.doi.org/10.1016/j.margeo.2005.11.006, 2006.

15   Bory, A., Dulac, F., Moulin, C., Chiapello, I., Newton, P., Guelle, W., Lambert, C., and Bergametti, G.: Atmospheric and oceanic dust fluxes in the northeastern tropical Atlantic Ocean: how close a coupling?, Annales Geophysicae, 2002, 2067-2076.

Cachier, H., Liousse, C., Buat-Menard, P., and Gaudichet, A.: Particulate content of savanna fire emissions, Journal of Atmospheric Chemistry, 22, 123-148, 1995.

20   Caquineau, S., Gaudichet, A., Gomes, L., and Legrand, M.: Mineralogy of Saharan dust transported over northwestern tropical Atlantic Ocean in relation to source regions, Journal of Geophysical Research: Atmospheres, 107, 2002.

Chiapello, I., Bergametti, G., Gomes, L., Chatenet, B., Dulac, F., Pimenta, J., and Santos Suares, E.: An additional low layer transport of Sahelian and Saharan dust over the north-eastern tropical Atlantic, Geophysical Research
25   Letters, 22, 3191-3194, 1995.

Chiapello, I., and Moulin, C.: TOMS and METEOSAT satellite records of the variability of Saharan dust transport over the Atlantic during the last two decades (1979–1997), Geophysical Research Letters, 29, 17-11-17-14, 10.1029/2001GL013767, 2002.

Deuser, W., Muller- Karger, F., and Hemleben, C.: Temporal variations of particle fluxes in the deep subtropical
30   and tropical North Atlantic: Eulerian versus Lagrangian effects, Journal of Geophysical Research: Oceans (1978–2012), 93, 6857-6862, 1988.

Fischer, G., and Wefer, G.: Long-term Observation of Particle Fluxes in the Eastern Atlantic: Seasonality, Changes of Flux with Depth and Comparison with the Sediment Record, in: The South Atlantic, Springer Berlin Heidelberg, 325-344, 1996.

35   Fischer, G., Karakas, G., Blaas, M., Ratmeyer, V., Nowald, N., Schlitzer, R., Helmke, P., Davenport, R., Donner, B., Neuer, S., and Wefer, G.: Mineral ballast and particle settling rates in the coastal upwelling system off NW Africa and the South Atlantic, International Journal of Earth Sciences, 10.1007/s00531-007-0234-7, 2007.

Fischer, G., and Karakas, G.: Sinking rates and ballast composition of particles in the Atlantic Ocean: implications for the organic carbon fluxes to the deep ocean, Biogeosciences, 6, 85-102, 2009.

40   Fischer, G., Reuter, C., Karakas, G., Nowald, N., and Wefer, G.: Offshore advection of particles within the Cape Blanc filament, Mauritania: Results from observational and modelling studies, Progress in Oceanography, 83, 322-330, http://dx.doi.org/10.1016/j.pocean.2009.07.023, 2009.

Fischer, G., Romero, O., Merkel, U., Donner, B., Iversen, M., Nowald, N., Ratmeyer, V., Ruhland, G., Klann, M., and Wefer, G.: Deep ocean mass fluxes in the coastal upwelling off Mauritania from 1988 to 2012: variability on
45   seasonal to decadal timescales, Biogeosciences, 13, 3071-3090, 10.5194/bg-13-3071-2016, 2016.

Fréon, P., Arístegui, J., Bertrand, A., Crawford, R. J. M., Field, J. C., Gibbons, M. J., Tam, J., Hutchings, L., Masski, H., Mullon, C., Ramdani, M., Seret, B., and Simier, M.: Functional group biodiversity in Eastern Boundary Upwelling Ecosystems questions the wasp-waist trophic structure, Progress in Oceanography, 83, 97-106, http://dx.doi.org/10.1016/j.pocean.2009.07.034, 2009.

5 Glaccum, R. A., and Prospero, J. M.: Saharan aerosols over the tropical North Atlantic - mineralogy, Marine Geology, 37, 295-321, 1980.

Goossens, D., and Offer, Z. Y.: Wind tunnel and field calibration of six aeolian dust samplers, Atmospheric Environment, 34, 1043-1057, 10.1016/s1352-2310(99)00376-3, 2000.

Goudie, A. S., and Middleton, N. J.: Saharan dust storms: nature and consequences, Earth-Science Reviews, 56,
10 179-204, 2001.

Griffin, D. W., Garrison, V. H., Herman, J. R., and Shinn, E. A.: African desert dust in the Caribbean atmosphere: Microbiology and public health, Aerobiologia, V17, 203-213, 2001.

Hamm, C. E.: Interactive aggregation and sedimentation of diatoms and clay-sized lithogenic material, Limnol. Oceanogr, 47, 1790-1795, 2002.

15 Huang, J., Zhang, C., and Prospero, J. M.: African dust outbreaks: A satellite perspective of temporal and spatial variability over the tropical Atlantic Ocean, Journal of Geophysical Research: Atmospheres (1984–2012), 115, 2010.

Ittekkot, V., Haake, B., Bartsch, M., Nair, R., and Ramaswamy, V.: Organic carbon removal in the sea: the continental connection, Geological Society, London, Special Publications, 64, 167-176, 1992.

20 Jickells, T. D., Dorling, S., Deuser, W. G., Church, T. M., Arimoto, R., and Prospero, J. M.: Air-borne dust fluxes to a deep water sediment trap in the Sargasso Sea, Global Biogeochemical Cycles, 12, 311-320, 10.1029/97GB03368, 1998.

Jickells, T. D., An, Z. S., Andersen, K. K., Baker, A. R., Bergametti, G., Brooks, N., Cao, J. J., Boyd, P. W., Duce, R. A., Hunter, K. A., Kawahata, H., Kubilay, N., laRoche, J., Liss, P. S., Mahowald, N., Prospero, J. M., Ridgwell,
25 A. J., Tegen, I., and Torres, R.: Global Iron Connections Between Desert Dust, Ocean Biogeochemistry, and Climate, Science, 308, 67-71, 2005.

Kaly, F., Marticorena, B., Chatenet, B., Rajot, J.-L., Janicot, S., Niang, A., Yahi, H., Thiria, S., Maman, A., and Zakou, A.: Variability of mineral dust concentrations over West Africa monitored by the Sahelian Dust Transect, Atmospheric Research, 164, 226-241, 2015.

30 Kandler, K., Schütz, L., Deutscher, C., Ebert, M., Hofmann, H., Jäckel, S., Jaenicke, R., Knippertz, P., Lieke, K., Massling, A., Petzold, A., Schladitz, A., Weinzierl, B., Wiedensohler, A., Zorn, S., and Weinbruch, S.: Size distribution, mass concentration, chemical and mineralogical composition and derived optical parameters of the boundary layer aerosol at Tinfou, Morocco, during SAMUM 2006, Tellus B, 61, 32-50, 10.1111/j.1600-0889.2008.00385.x, 2009.

35 Kandler, K., Schütz, L., Jäckel, S., Lieke, K., Emmel, C., Müller- Ebert, D., Ebert, M., Scheuvens, D., Schladitz, A., and Šegvić, B.: Ground- based off- line aerosol measurements at Praia, Cape Verde, during the Saharan Mineral Dust Experiment: microphysical properties and mineralogy, Tellus B, 63, 459-474, 2011.

Klaas, C., and Archer, D. E.: Association of sinking organic matter with various types of mineral ballast in the deep sea: Implications for the rain ratio, Global Biogeochem. Cycles, 16, 1116, 10.1029/2001gb001765, 2002.

40 Knappertsbusch, M., and Brummer, G.-J.: A sediment trap investigation of sinking coccolithophorids in the North Atlantic, Deep Sea Research Part I: Oceanographic Research Papers, 42, 1083-1109, 1995.

Knauer, G., and Asper, V.: Sediment Trap Technology and Sampling, U.S. Global Ocean Flux Study, 1989.

Koning, E., Epping, E., and Van Raaphorst, W.: Determining biogenic silica in marine samples by tracking silicate and aluminium concentrations in alkaline leaching solutions, Aquatic Geochemistry, 8, 37-67, 2002.

Liu, Z., Omar, A., Vaughan, M., Hair, J., Kittaka, C., Hu, Y., Powell, K., Trepte, C., Winker, D., Hostetler, C., Ferrare, R., and Pierce, R.: CALIPSO lidar observations of the optical properties of Saharan dust: A case study of long-range transport, Journal of Geophysical Research: Atmospheres, 113, n/a-n/a, 10.1029/2007JD008878, 2008.

5   Maher, B. A., Prospero, J. M., Mackie, D., Gaiero, D., Hesse, P. P., and Balkanski, Y.: Global connections between aeolian dust, climate and ocean biogeochemistry at the present day and at the last glacial maximum, Earth-Science Reviews, 99, 61-97, DOI: 10.1016/j.earscirev.2009.12.001, 2010.

Mahowald, N., Albani, S., Kok, J. F., Engelstaeder, S., Scanza, R., Ward, D. S., and Flanner, M. G.: The size distribution of desert dust aerosols and its impact on the Earth system, Aeolian Research, 15, 53-71, http://dx.doi.org/10.1016/j.aeolia.2013.09.002, 2014.

10 Marticorena, B., Chatenet, B., Rajot, J.-L., Traoré, S., Coulibaly, M., Diallo, A., Koné, I., Maman, A., NDiaye, T., and Zakou, A.: Temporal variability of mineral dust concentrations over West Africa: analyses of a pluriannual monitoring from the AMMA Sahelian Dust Transect, Atmos. Chem. Phys., 10, 8899-8915, 2010.

Mortlock, R. A., and Froelich, P. N.: A simple method for the rapid determination of biogenic opal in pelagic marine sediments, Deep Sea Research, A 36, 1415 - 1426, 1989.

15 Mulitza, S., Prange, M., Stuut, J.-B. W., Zabel, M., von Dobeneck, T., Itambi, A. C., Nizou, J., Schulz, M., and Wefer, G.: Sahel megadroughts triggered by glacial slowdowns of Atlantic meridional overturning, Paleoceanography, 23, doi:10.1029/2008PA001637, 10.1029/2008PA001637, 2008.

Neuer, S., Freudenthal, T., Davenport, R., Llinás, O., and Rueda, M.-J.: Seasonality of surface water properties and particle flux along a productivity gradient off NW Africa, Deep Sea Research Part II: Topical Studies in
20 Oceanography, 49, 3561-3576, 2002.

Nowald, N., Iversen, M. H., Fischer, G., Ratmeyer, V., and Wefer, G.: Time series of in-situ particle properties and sediment trap fluxes in the coastal upwelling filament off Cape Blanc, Mauritania, Progress in Oceanography, 137, Part A, 1-11, http://dx.doi.org/10.1016/j.pocean.2014.12.015, 2015.

Prospero, J. M., Bonatti, E., Schubert, C., and Carlson, T. N.: Dust in the Caribbean atmosphere traced to an
25 African dust storm, Earth and Planetary Science Letters, 9, 287-293, 1970.

Prospero, J. M., Glaccum, R. A., and Nees, R. T.: Atmospheric transport of soil dust from Africa to South America, Nature, 289, 570-572, 1981.

Prospero, J. M., and Lamb, P. J.: African droughts and dust transport to the Caribbean: climate change implications, Science, 302, 1024-1027, 2003.

30 Prospero, J. M., Collard, F.-X., Molinie, J., and Jeannot, A.: Characterizing the annual cycle of African dust transport to the Caribbean Basin and South America and its impact on the environment and air quality, Global Biogeochemical Cycles, 28, 757-773, 10.1002/2013gb004802, 2014.

Pye, K.: Aeolian dust and dust deposits, Academic Press, London, 334 pp., 1987.

Ratmeyer, V., Balzer, W., Bergametti, G., Chiapello, I., Fischer, G., and Wyputta, U.: Seasonal impact of mineral
35 dust on deep-ocean particle flux in the eastern subtropical Atlantic Ocean, Marine Geology, 159, 241-252, 1999a.

Ratmeyer, V., Fischer, G., and Wefer, G.: Lithogenic particle fluxes and grain size distributions in the deep ocean off northwest Africa: Implications for seasonal changes of aeolian dust input and downward transport, Deep Sea Research Part I: Oceanographic Research Papers, 46, 1289-1337, 1999b.

Richter, T. O., Van der Gaast, S., Koster, B., Vaars, A., Gieles, R., de Stigter, H. C., De Haas, H., and van Weering,
40 T. C.: The Avaatech XRF Core Scanner: technical description and applications to NE Atlantic sediments, Geological Society, London, Special Publications, 267, 39-50, 2006.

Scheuvens, D., Schütz, L., Kandler, K., Ebert, M., and Weinbruch, S.: Bulk composition of northern African dust and its source sediments — A compilation, Earth-Science Reviews, 116, 170-194, http://dx.doi.org/10.1016/j.earscirev.2012.08.005, 2013.

45 Schlitzer, R.: Ocean Data View, 2015.

Siegel, D. A., and Deuser, W. G.: Trajectories of sinking particles in the Sargasso Sea: modeling of statistical funnels above deep-ocean sediment traps, Deep Sea Research Part I: Oceanographic Research Papers, 44, 1519-1541, http://dx.doi.org/10.1016/S0967-0637(97)00028-9, 1997.

Skonieczny, C., Bory, A., Bout- Roumazeilles, V., Abouchami, W., Galer, S., Crosta, X., Stuut, J. B., Meyer, I., Chiapello, I., and Podvin, T.: The 7–13 March 2006 major Saharan outbreak: Multiproxy characterization of mineral dust deposited on the West African margin, Journal of Geophysical Research: Atmospheres, 116, 2011.

Skonieczny, C., Bory, A., Bout-Roumazeilles, V., Abouchami, W., Galer, S. J. G., Crosta, X., Diallo, A., and Ndiaye, T.: A three-year time series of mineral dust deposits on the West African margin: Sedimentological and geochemical signatures and implications for interpretation of marine paleo-dust records, Earth and Planetary Science Letters, 364, 145-156, http://dx.doi.org/10.1016/j.epsl.2012.12.039, 2013.

Stuut, J.-B. W., Zabel, M., Ratmeyer, V., Helmke, P., Schefuß, E., Lavik, G., and Schneider, R. R.: Provenance of present-day eolian dust collected off NW Africa, Journal of Geophysical Research, 110, 10.1029/2004JD005161, 2005.

Stuut, J.-B. W., Boersen, B., Brück, H. M., Hansen, A., Koster, B., Van der Does, M., and Witte, Y.: TRAFFIC: Transatlantic fluxes of Saharan dust, Leitstelle Deutsche Forschungsschiffe, Hamburg, 28; available at http://melia.nioz.nl/public/dmg/rpt/crs/m89.pdf, 2012.

Stuut, J.-B. W., Brummer, G. J. A., van der Does, M., Friese, C., Geerken, E., van der Heide, R., Korte, L., Koster, B., Metcalfe, B., Munday, C. I., van Ooijen, J., Siccha, M., Veldhuizen, R., de Visser, J.-D., Witte, Y., and and Wuis, L.: Cruise Report RV Pelagia 64PE378, TRAFFIC II: Transatlantic Fluxes of Saharan Dust. 9 November - 6 December 2013, 2013. available at http://melia.nioz.nl/public/dmg/rpt/crs/64pe378.pdf
Subramaniam, A., Yager, P., Carpenter, E., Mahaffey, C., Björkman, K., Cooley, S., Kustka, A., Montoya, J., Sañudo-Wilhelmy, S., and Shipe, R.: Amazon River enhances diazotrophy and carbon sequestration in the tropical North Atlantic Ocean, Proceedings of the National Academy of Sciences, 105, 10460-10465, 2008.

Thunell, R., Benitez-Nelson, C., Varela, R., Astor, Y., and Muller-Karger, F.: Particulate organic carbon fluxes along upwelling-dominated continental margins: Rates and mechanisms, Global Biogeochemical Cycles, 21, 10.1029/2006gb002793, 2007.

Tjallingii, R., Röhl, U., Kölling, M., and Bickert, T.: Influence of the water content on X- ray fluorescence core-scanning measurements in soft marine sediments, Geochemistry, Geophysics, Geosystems, 8, 2007.

Tsamalis, C., Chédin, A., Pelon, J., and Capelle, V.: The seasonal vertical distribution of the Saharan Air Layer and its modulation by the wind, Atmos. Chem. Phys., 13, 11235-11257, 10.5194/acp-13-11235-2013, 2013.

Van der Does, M., Korte, L. F., Munday, C. I., Brummer, G. J. A., and Stuut, J. B. W.: Particle size traces modern Saharan dust transport and deposition across the equatorial North Atlantic, Atmos. Chem. Phys., 16, 13697-13710, 10.5194/acp-16-13697-2016, 2016.

Van Raaphorst, W., Malschaert, H., van Haren, H., Boer, W., and Brummer, G.-J.: Cross-slope zonation of erosion and deposition in the Faeroe-Shetland Channel, North Atlantic Ocean, Deep Sea Research Part I: Oceanographic Research Papers, 48, 567-591, http://dx.doi.org/10.1016/S0967-0637(00)00052-2, 2001.

Waniek, J., Koeve, W., and Prien, R. D.: Trajectories of sinking particles and the catchment areas above sediment traps in the northeast Atlantic, Journal of Marine Research, 58, 983-1006, 2000.

Wefer, G., and Fischer, G.: Seasonal patterns of vertical particle flux in equatorial and coastal upwelling areas of the eastern Atlantic, Deep Sea Research Part I: Oceanographic Research Papers, 40, 1613-1645, http://dx.doi.org/10.1016/0967-0637(93)90019-Y, 1993.

Weltje, G. J., and Tjallingii, R.: Calibration of XRF core scanners for quantitative geochemical logging of sediment cores: theory and application, Earth and Planetary Science Letters, 274, 423-438, 2008.

Yeung, L. Y., Berelson, W. M., Young, E. D., Prokopenko, M. G., Rollins, N., Coles, V. J., Montoya, J. P., Carpenter, E. J., Steinberg, D. K., and Foster, R. A.: Impact of diatom- diazotroph associations on carbon export in the Amazon River plume, Geophysical Research Letters, 39, 2012.

Yu, H., Chin, M., Bian, H., Yuan, T., Prospero, J. M., Omar, A. H., Remer, L. A., Winker, D. M., Yang, Y., Zhang, Y., and Zhang, Z.: Quantification of trans-Atlantic dust transport from seven-year (2007–2013) record of CALIPSO lidar measurements, Remote Sensing of Environment, 159, 232-249, http://dx.doi.org/10.1016/j.rse.2014.12.010, 2015.